

JGR Space Physics

RESEARCH ARTICLE

10.1029/2025JA033760

Key Points:

- Foreshock and ground-based ultralow frequency (ULF) wave power are power law correlated with coefficients of >0.5 at ~ 30 s period
- The statistical relationship between the two ULF wave types depends on frequency, magnetic latitude, and magnetic local time
- Transmission of ULF waves is better correlated with local bow shock geometry than interplanetary magnetic field cone angle

Supporting Information:

Supporting Information may be found in the online version of this article.

Correspondence to:

T. Z. Liu,
terryliuzixu@ucla.edu

Citation:

Liu, T. Z., Angelopoulos, V., Dorfman, S., Hartinger, M. D., Zhang, K., Raptis, S., & Ma, D. (2025). Statistical relationship between foreshock ULF wave power and ground-based Pc3-4 wave power. *Journal of Geophysical Research: Space Physics*, 130, e2025JA033760. <https://doi.org/10.1029/2025JA033760>




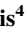


Received 17 JAN 2025
Accepted 21 AUG 2025

Author Contributions:

Conceptualization: Terry Zixu Liu
Data curation: Terry Zixu Liu
Formal analysis: Terry Zixu Liu
Funding acquisition: Kun Zhang
Investigation: Terry Zixu Liu, Vassilis Angelopoulos, Seth Dorfman, Michael D. Hartinger, Kun Zhang, Savvas Raptis, Donglai Ma
Methodology: Terry Zixu Liu, Vassilis Angelopoulos, Seth Dorfman
Resources: Terry Zixu Liu
Supervision: Vassilis Angelopoulos
Validation: Terry Zixu Liu
Visualization: Terry Zixu Liu
Writing – original draft: Terry Zixu Liu
Writing – review & editing: Terry Zixu Liu, Vassilis Angelopoulos, Seth Dorfman, Michael D. Hartinger, Savvas Raptis

© 2025. American Geophysical Union. All Rights Reserved.

Statistical Relationship Between Foreshock ULF Wave Power and Ground-Based Pc3-4 Wave Power

Terry Zixu Liu¹ , Vassilis Angelopoulos¹, Seth Dorfman^{2,3} , Michael D. Hartinger^{1,2} , Kun Zhang¹ , Savvas Raptis⁴ , and Donglai Ma¹ 

¹Department of Earth, Planetary, and Space Sciences, University of California, Los Angeles, CA, USA, ²Space Science Institute, Boulder, CO, USA, ³Department of Physics and Astronomy, University of California, Los Angeles, CA, USA, ⁴Applied Physics Laboratory, Johns Hopkins University, Baltimore, MD, USA

Abstract Magnetospheric ultralow frequency (ULF) waves are fundamental for coupling energy across the magnetosphere and ionosphere. Pc3-4 waves (7–100 mHz) are associated with small interplanetary magnetic field (IMF) cone angles, suggesting that foreshock ULF waves are the source. To understand the relationship between foreshock and magnetospheric ULF waves, we perform a statistical study using the THEMIS spacecraft to observe foreshock ULF waves and ground magnetometers (GMAG) to infer magnetospheric ULF waves. We observe a power law correlation between foreshock and ground-based ULF wave power, with correlation coefficients exceeding 0.5 around the typical period of foreshock “30s waves” in contrast to correlation coefficients ~ 0.3 between solar wind and ground-based ULF wave power. The power law parameters decrease with lower magnetic latitudes, indicating weaker power transport deeper in the magnetosphere. Additionally, the correlation coefficients decrease with larger magnetic local time (MLT) separation between the THEMIS spacecraft and GMAG. We also find that ground-based Pc3-4 wave power exhibits a stronger dependence on the local bow shock θ_{Bn} (angle between the shock normal and the IMF) than on the IMF cone angle. These findings indicate that foreshock ULF waves are more likely to be transmitted from the local MLT than across the subsolar point. We also find that ground-based Pc3-4 waves show a stronger dependence on the solar wind speed than do foreshock ULF waves, suggesting a possible contribution from Kelvin-Helmholtz instability and shock-generated transients. Our results provide new insights into the connection between foreshock ULF waves and ground-based Pc3-4 waves.

1. Introduction

Ultralow frequency (ULF) waves are a fundamental element in the magnetosphere, which were initially identified through ground-based measurements and later supplemented by spacecraft observations (see review by Takahashi et al., 2006). They play a crucial role in energy transport and coupling across various scales. Their broad frequency range (~ 1 mHz–10 Hz) was subdivided into shorter bands based on their origins and properties (Jacobs et al., 1964). For example, Pc5 waves (~ 1 –7 mHz) can be driven by direct penetration of solar wind dynamic pressure variations, eigenmode oscillations driven by solar wind disturbances, or the Kelvin-Helmholtz (KH) instability, whereas Pc1-2 waves (0.1–5 Hz) typically arise from internal sources, such as cyclotron resonance with energetic ring current ions (see review by Menk, 2011).

As for Pc3-4 waves (7–100 mHz), previous statistical studies have shown that they more likely occur under smaller interplanetary magnetic field (IMF) cone angles (e.g., Greenstadt & Olson, 1976; Russell et al., 1983; Takahashi et al., 1984), implying that foreshock ULF waves at the subsolar bow shock are the source. When the IMF is quasi-parallel to the bow shock normal, some of the solar wind ions are reflected, forming the ion foreshock (see review by Eastwood et al., 2005). The counter-streaming between foreshock ions and solar wind ions excites foreshock ULF waves, including the commonly observed “30s waves” (see review by Wilson, 2016). These waves are convected by the supermagnetosonic solar wind across the bow shock and then propagate earthward in the magnetosheath toward the magnetopause (Turc et al., 2023). The period of 30s waves depends on the ion cyclotron frequency which is proportional to the IMF strength, and the frequency of magnetospheric Pc3-4 waves shows a similar IMF dependence, suggesting that 30s waves are the source of the magnetospheric perturbations (e.g., Russell & Hoppe, 1981, 1983). Additionally, magnetospheric Pc3-4 wave power is correlated with the solar wind velocity, favoring another possibility that the KH instability could be the source (e.g., Golikov et al., 1983; Singer et al., 1977; Wolfe et al., 1980). However, fast solar wind velocity can also lead to fast

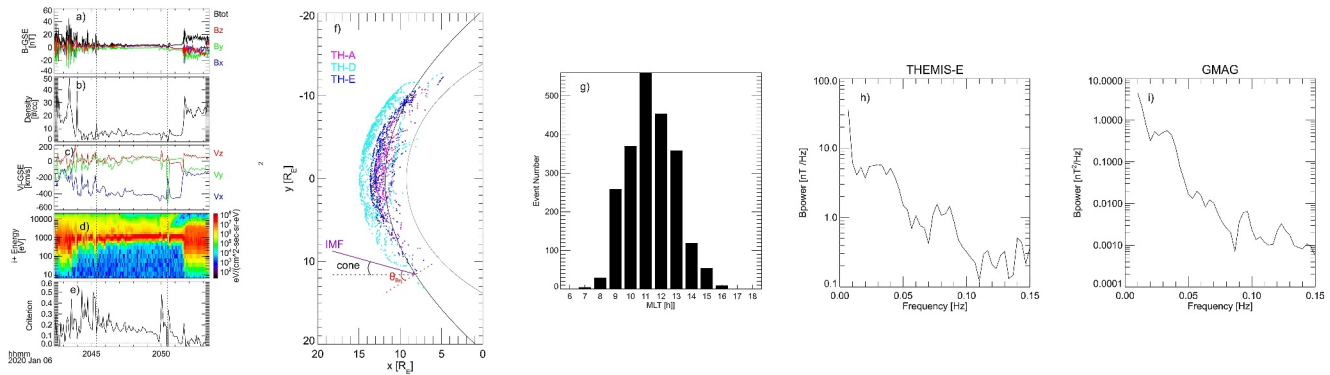


Figure 1. THEMIS-E observation of foreshock ultralow frequency waves at magnetic local time (MLT) of 9.6 hr: (a) magnetic field in GSE, (b) density, (c) ion bulk velocity in GSE, (d) ion energy spectrum, and (e) $\Delta \log(E_i) - \Delta \log(E_i)'$ described in the text. Vertical dotted lines indicate the foreshock time window based on the criteria. Panel (f) shows the spatial distribution of foreshock events observed by three THEMIS spacecraft. The cone angle between the interplanetary magnetic field (IMF) and GSE-X (black) and θ_{Bn} between the IMF and local bow shock normal (red) are sketched. The Merka et al. (2005) bow shock model and Shue et al. (1998) magnetopause model are used. Panel (g) shows the number distribution of MLT of foreshock events. Panel (h) is the foreshock wave power spectrum in the time window. Panel (i) shows the magnetospheric wave power spectrum remotely sensed by ground magnetometers stations at MLT of 10.1 hr and magnetic latitudes of 55.4°.

foreshock ion velocity (see review by Burgess et al., 2012), providing more free energy for foreshock ULF waves. Thus, whether foreshock ULF waves or the KH instability drive magnetospheric Pc3-4 waves has been debated.

Later, case studies by Engebretson et al. (1987) showed simultaneous observations of foreshock ULF waves and magnetospheric Pc3-4 waves, confirming their connection. These case studies suggested that foreshock ULF waves could enter the magnetosphere more likely through the cusp (Lanzerotti et al., 1981) than across the subsolar magnetopause (Verzari, 1973). Case studies by Verö et al. (1998) identified the relationship between field line resonances and magnetospheric ULF waves driven by the upstream waves. Conjunction observations by Clausen et al. (2009) provided the first simultaneous observations of ULF waves in the foreshock, in the magnetosphere, and on the ground. Takahashi et al. (2021) observed the transmission of foreshock ULF waves during a magnetic cloud.

Despite several case studies demonstrating a direct connection between foreshock ULF waves and magnetospheric Pc3-4 waves, a comprehensive statistical study of this connection is still missing. Additionally, case studies can be complicated by the properties of energy sources and magnetospheric resonators, and statistical studies could help mitigate these effects (Harteringer et al., 2023). Since 2016, the Time History of Events and Macroscale Interactions during Substorms (THEMIS, Angelopoulos, 2008) spacecraft has been frequently in the upstream region, providing a rich database of foreshock ULF waves in the equatorial plane. Through the conjunction between the THEMIS spacecraft to observe foreshock ULF waves and ground magnetometers (GMAG) to remotely infer magnetospheric ULF waves, we obtain a sufficient data set to statistically analyze the connection between them. The data set is described in Section 2, with results presented in Section 3, followed by discussion and summary in Sections 4 and 5.

2. Data and Methods

Since 2016, three THEMIS spacecraft (TH-A, TH-D, and TH-E) have frequently entered the upstream region with an apogee of $\sim 13 R_E$. We utilize magnetic field data from the fluxgate magnetometer (FGM; Auster et al., 2008) and plasma data from the electrostatic analyzer (ESA; McFadden et al., 2008) onboard THEMIS for foreshock ULF waves. We use GMAG stations from several networks obtained from the THEMIS and NASA CDAWeb repositories, including THEMIS (UCLA) GMAG data (Russell et al., 2009) as well as other GMAG networks (e.g., CARISMA and USGS) with 1s resolution to infer magnetospheric ULF waves.

When the three THEMIS spacecraft were in the upstream region in fast survey mode from 2016 to 2020, we identified the time intervals of ion foreshock (e.g., Figure 1) based on the presence of foreshock ions in the ion energy spectrum (e.g., yellow and green part in Figure 1d above the red solar wind ion beam). Below are the detailed identification processes:

We first visually identified 1-hr time windows where spacecraft reached upstream regions in fast-survey mode. For these 1-hr time windows, we used an automatic method to identify foreshock time intervals based on the following criteria:

1. The x component of the ion bulk velocity should be faster than 260 km/s in the anti-sunward direction to avoid (transient) magnetosheath time intervals and foreshock transient phenomena (e.g., at two vertical dotted lines in Figure 1; see review by Zhang et al. (2022)).
2. We used energy flux-weighted energy to identify foreshock time intervals. We first calculated $\log(\bar{E}) = \sum_i F_i \cdot \log(E_i) / \sum_i F_i$, where F_i is energy flux of i th energy channel at energy E_i . Because the energy flux of solar wind ions is dominant, \bar{E} is nearly solar wind ion energy. We then calculated $\Delta\log(E_i) = \log(E_i/\bar{E})$ and $\Delta\log(\bar{E}) = \sqrt{\sum_i F_i \cdot \Delta\log(E_i)^2 / \sum_i F_i}$. We used log scales because ESA energy channels are distributed on log scales so that $\Delta\log(E_i)$ are evenly distributed. The meaning of $\Delta\log(\bar{E})$ is how significantly the energy flux-weighted energy deviates from solar wind energy due to foreshock ions. We repeated the same process for energy flux in the anti-sunward direction (spacecraft phi angle from 165° to 195° to minimize foreshock ion flux), $\Delta\log(\bar{E})'$, as a reference. Through tests, we found that $\Delta\log(E_i) - \Delta\log(\bar{E})' > 0.03$ can identify most of foreshock time intervals (see Figure 1e that the criterion value roughly correlates with the intensity of non-solar wind ions).
3. The foreshock time intervals should be longer than 5 min. If a foreshock time interval spans portions of two adjacent 1-hr time windows, we only use the time interval at the leading edge of the time window to avoid duplicate counts (see example in Figure S1 in Supporting Information S1).

The list of 2218 foreshock time intervals can be found in the Supporting Information S1. More examples can be found in Figure S1 in Supporting Information S1 with limitations of identification processes discussed in the Supporting Information S1. The locations of foreshock events span from 8 to 16hr magnetic local time (MLT) with a dawn-dusk asymmetry in event numbers due to Parker spiral geometry (Figures 1f and 1g).

For each foreshock time interval, we calculate magnetic power spectra (sum of all three components) using a 5-min sliding window with a 2.5-min time step. Figure 1h illustrates an example of a wave power spectrum with a bump at ~ 0.03 Hz corresponding to the commonly observed 30s waves (another bump at ~ 0.08 Hz could be 10s waves).

The duration of foreshock time intervals varies partly depending on spacecraft orbits and the stability of the bow shock and the IMF. If we use wave power spectra from every time window (when foreshock time interval is longer than 7.5 min), the results will be unphysically weighted toward time intervals where the spacecraft spends longer in the ion foreshock. To address this potential sampling bias, we use only the central time window for each foreshock time interval. Additionally, one foreshock time interval could be observed by multiple spacecraft (~ 200 events). Because foreshock properties vary along the bow shock normal and curved bow shock surface, with spacecraft separation even less than 1 R_E (25 events), clear differences are observed (see examples in Figure S2 in Supporting Information S1). We thus consider the foreshock time interval observed by multiple spacecraft as separate events under different upstream parameters at different MLT.

For each foreshock time window, we then calculate wave power spectra using GMAG stations located at longitudes within ± 6 hr MLT relative to the spacecraft (using all three components). Figure 1i illustrates an example of a wave power spectrum measured by GMAG stations located at longitudes ~ 0.5 hr MLT away from the spacecraft. It also shows a bump at ~ 0.03 Hz. Due to 1s resolution requirement, available GMAG stations are located mostly in North America. Because of this limited coverage, $\sim 53\%$ of foreshock events do not have available GMAG stations (see probability distribution of GMAG station numbers and spatial distribution of available GMAG stations in Figure S3 in Supporting Information S1).

At each frequency, we calculate Spearman correlation coefficients (which assesses monotonic relationships) between foreshock wave power and ground-based wave power across foreshock events. We classify correlation strengths as follows: 0.6–0.8 as strong, 0.4–0.6 as moderate, 0.2–0.4 as weak, and 0–0.2 as no correlation. We then examine how various parameters affect correlation.

For comparison, we repeat the same analysis for the solar wind wave power. The solar wind time intervals are selected using similar criteria except that $\Delta\log(E_i) - \Delta\log(\bar{E})' < 0.02$, and we manually remove identified time

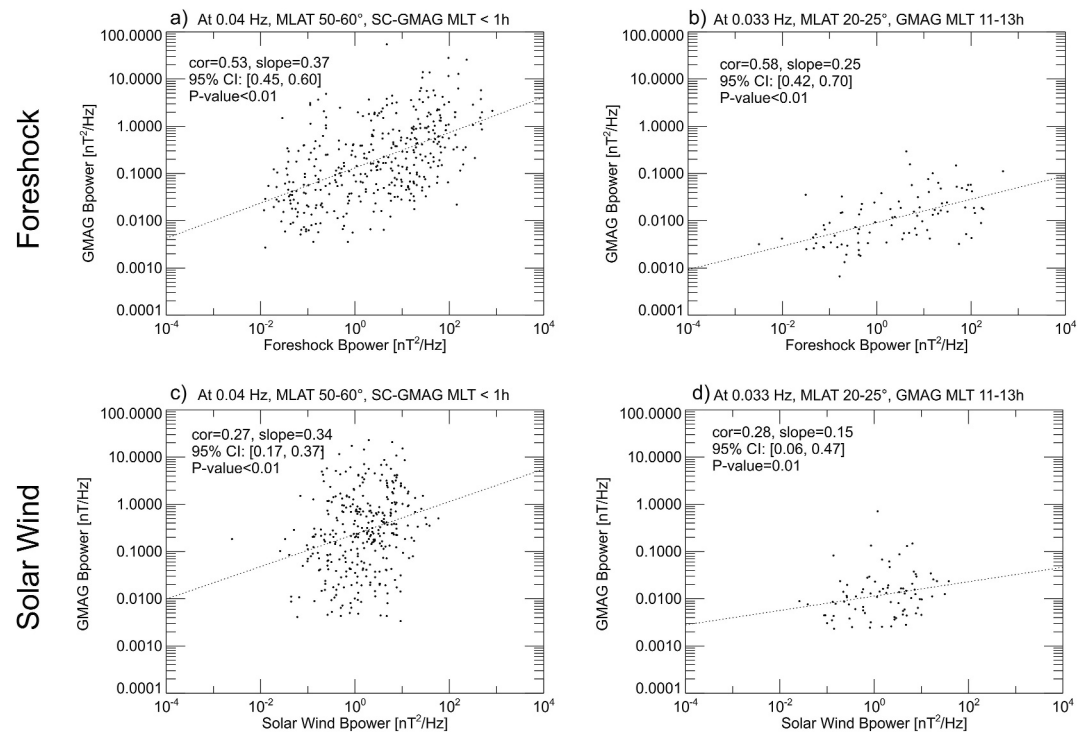


Figure 2. Foreshock ultralow frequency (ULF) wave power observed by the THEMIS spacecraft versus ground-based ULF wave power remotely sensed by ground magnetometers (GMAG) stations (a) at frequency of 0.04 Hz and GMAG magnetic latitudes (MLAT) of 50–60° with magnetic local time (MLT) separation from the THEMIS spacecraft less than 1 hr, and (b) at frequency of 0.033 Hz and GMAG MLAT of 20–25° with GMAG MLT from 11 to 13hr. Panels (c) and (d) are in the same format as panels (a) and (b) except for solar wind ULF wave power. Spearman correlation coefficient, slope, 95% confidence interval, and *P*-value are labeled in each panel.

intervals that include weak foreshock ions. The solar wind time intervals must be separated by at least 30 min to avoid duplication (because qualitatively similar solar wind time intervals are often separated by multiple transient foreshock time intervals). A total of 1,065 solar wind time intervals are selected. The solar wind events exhibit only slight dawn-dusk asymmetry in their MLT distribution and mainly occur under large IMF cone angles (70° on average), as expected.

The angle between the local bow shock normal and the IMF (θ_{Bn}) is a critical parameter in foreshock dynamics (see sketch in Figure 1f). To calculate θ_{Bn} , we use the Merka et al. (2005) bow shock model with input from time-averaged parameters measured by the THEMIS spacecraft. The spacecraft position is projected along the radial direction to the model bow shock to obtain the local bow shock normally. Although projection along the IMF is a more physical method, we do not use it in this study because the upstream spacecraft is frequently downstream of the model bow shock due to model uncertainties, leading to incorrect projection directions. For foreshock and solar wind events, the average θ_{Bn} is $\sim 37^\circ$ and $\sim 70^\circ$, respectively.

3. Results

To compare the power spectra of foreshock and ground-based ULF waves, we examine the correlation between their wave powers across different frequencies, MLT, and magnetic latitudes (MLAT) of GMAG stations. We also examine how upstream parameters affect both foreshock and ground-based ULF wave power at various frequencies.

3.1. Statistical Relationship of Wave Power

Before we examine the dependence on each parameter, we first show two examples under sets of parameters where the correlation coefficients are among the highest. Figure 2a compares foreshock and ground-based ULF wave power at 0.04 Hz using GMAG stations with MLAT of 50–60° and MLT separation from the spacecraft

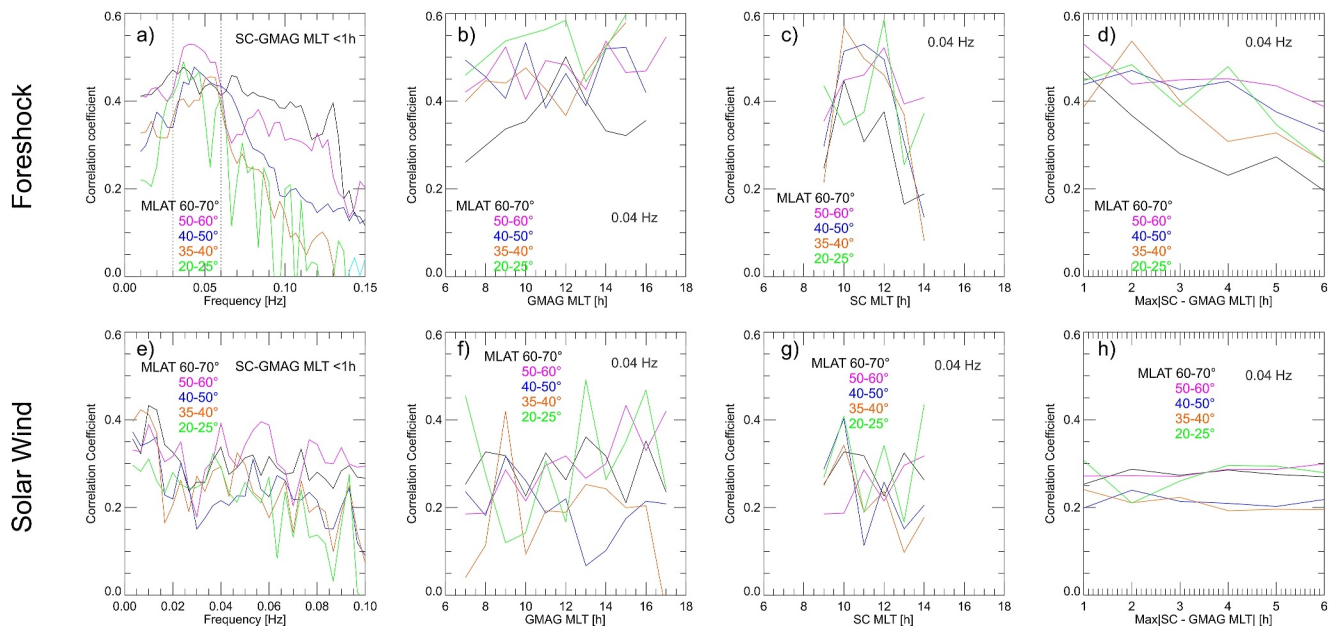


Figure 3. The Spearman correlation coefficient between the foreshock and ground-based ultralow frequency (ULF) wave power versus (a) frequency with magnetic local time (MLT) separation between the THEMIS spacecraft and ground magnetometers (GMAG) stations less than 1 hr, (b) the MLT of GMAG stations at 0.04 Hz (without MLT separation limitation for more data points), (c) the MLT of spacecraft at 0.04 Hz (without MLT separation limitation for more data points), and (d) the MLT separation between the THEMIS spacecraft and GMAG stations with cadence of 1 hr at 0.04 Hz. Different colors represent different magnetic latitudes ranges. Panels (e)–(h) are in the same format as panels (a)–(d) except for solar wind ULF wave power.

less than 1 hr. A power law relationship (which manifests as a linear relationship on log-log scales) is evident, with a Spearman correlation coefficient of ~ 0.53 (Pearson correlation coefficient, for linear relationship, shows similar results on log-log scales) and a slope of 0.37 on log-log scales. Figure 2b shows another comparison at 0.033 Hz using GMAG stations with MLAT of 20° – 25° and MLT of 11–13 hr. There are fewer data points due to fewer GMAG stations at low MLAT, but a power law relationship is also clearly seen with a correlation coefficient of ~ 0.58 and a slope of 0.25 on log-log scales. These results suggest that the contribution from foreshock ULF wave power P_f to ground-based ULF wave power P_m can be written as $P_m = a \cdot P_f^b$, where factors a and b can be fitted through linear regression on log-log scales. In contrast, under the same parameter sets, solar wind ULF wave power shows a weak correlation with ground-based ULF wave power (Figures 2c and 2d).

Next, we determine how frequency, MLAT, and MLT affect the correlation coefficients and fitted factors. Figure 3a shows that the highest correlation coefficients between foreshock and ground-based ULF wave power are within the 0.03–0.06 Hz frequency range across various MLAT, suggesting that foreshock 30s waves are an important source of magnetospheric ULF waves even at MLAT as low as 20° – 25° . In comparison, the correlation coefficients between solar wind and ground-based ULF wave power tend to increase up to ~ 0.4 with decreasing frequency (Figure 3e), consistent with previous studies that indicate that solar wind is a typical driver of Pc5 waves (~ 1 – 7 mHz; e.g., Bentley et al., 2018; Eriksson et al., 2006; Stephenson & Walker, 2002). Outside the 0.03–0.06 Hz frequency range, the correlation coefficients between foreshock and ground-based ULF wave power are comparable to the solar-wind level, indicating the possible role of background solar wind waves. We thus focus on the frequency of foreshock 30s waves, for example, 0.04 Hz, where the correlation coefficient peak.

Figure 3b shows that the correlation coefficients between foreshock and ground-based ULF wave power at 0.04 Hz do not clearly depend on the MLT of GMAG stations except for MLAT of 60° – 70° (other frequencies around 0.04 Hz show similar profiles). Figure 3c shows that the correlation coefficients peak when the spacecraft MLT is ~ 10 – 12 hr. This dawn-dusk asymmetry is partly due to insufficient event numbers on the duskside (see MLT distribution of foreshock events in Figure 1g) caused by Parker spiral geometry, and this asymmetry is weaker and smoother when we increase MLT bin size from 1 to 2 hr for larger event numbers (see Figure S4 in Supporting Information S1). Additionally, Figure 3d shows a trend that the correlation coefficients at 0.04 Hz decrease with larger MLT separation between the THEMIS spacecraft and GMAG stations (other frequencies

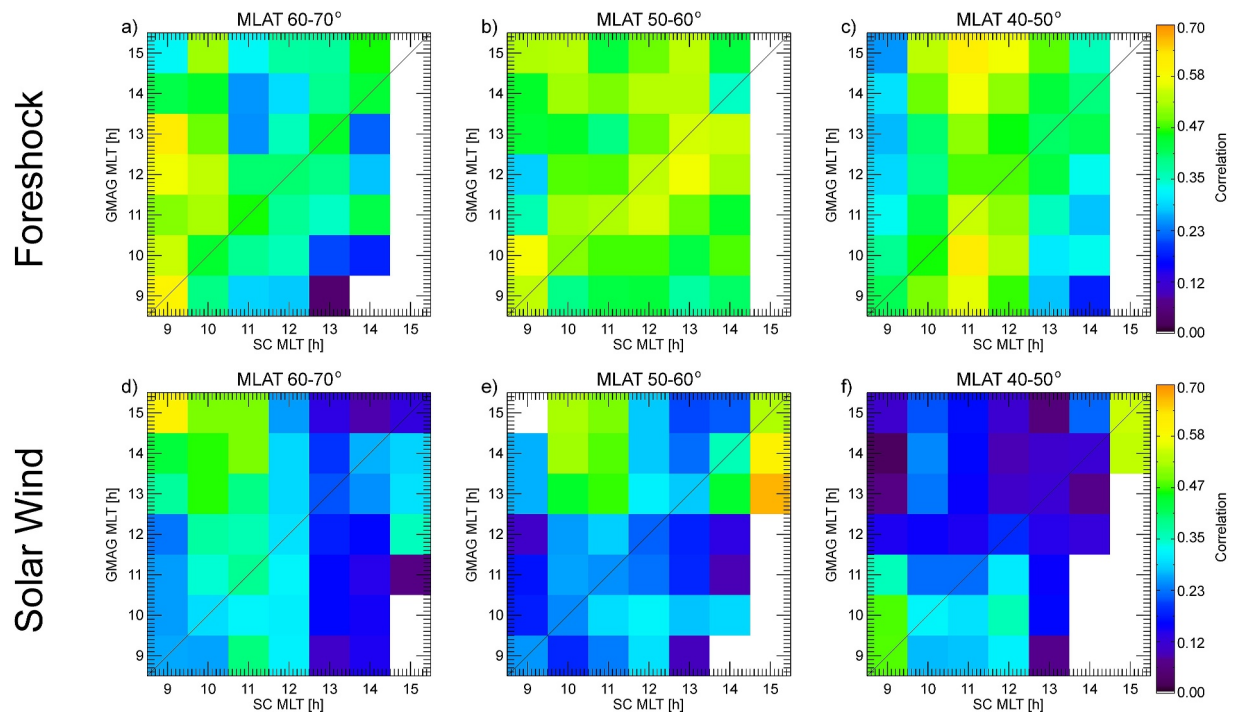


Figure 4. Spearman correlation coefficients as a function of THEMIS spacecraft magnetic local time (MLT) and ground magnetometers (GMAG) station MLT, at 0.04 Hz, for foreshock events (top) and solar wind events (bottom). GMAG stations below 40° magnetic latitudes are excluded because of limited coverage at lower latitudes. The bins are separated by 1 hr MLT with a size of 2 hr MLT \times 2 hr MLT. The bins with event numbers below 20 are removed.

around 0.04 Hz show similar trends). Solar wind events, on the other hand, do not show clear dependence on MLT (Figures 3f–3h) since solar wind impacts are global. These results suggest that foreshock ULF waves are transmitted into the magnetosphere more likely around the local MLT rather than at the subsolar point. Especially, because of the Parker spiral geometry, foreshock ULF waves can be transmitted more frequently on the dawnside than on the duskside, consistent with previous studies (e.g., Takahashi & Anderson, 1992; Turc et al., 2022).

To further examine the MLT dependence of wave transmission, Figure 4 shows correlation coefficients as a function of both GMAG station and spacecraft MLTs at 0.04 Hz. The bin size is 2 hr MLT \times 2 hr MLT, with a 1 hr MLT resolution (resulting in overlapping bins). We include GMAG stations located at MLAT above 40° because of more limited coverage at lower MLAT. For foreshock events, Figures 4a–4c generally show stronger correlation along the diagonal (black line), consistent with Figure 3d that indicates stronger correlation for smaller MLT separations. Additional MLT-dependent features also appear. In Figure 4a, the correlation peaks when the THEMIS spacecraft is located at ~9–10 hr MLT and GMAG stations are near noon. This likely corresponds to the 12 hr MLT peak for GMAG stations in Figure 3b and the 10 hr MLT peak for THEMIS spacecraft in Figure 3c and Figure S4 in Supporting Information S1 (black lines). In Figure 4b, the correlation is stronger when GMAG stations are located at ~14–15 hr MLT. In Figure 4c, the correlation peaks when the THEMIS spacecraft is at 11 hr MLT, spanning a broad MLT range for GMAG stations, except at ~12 hr (corresponding to the blue line in Figure 3c and Figure S4 in Supporting Information S1). These results suggest the presence of multiple transmission mechanisms, including localized transmission preferentially within ± 1 hr MLT and broader-range transmission across a few hours of MLT. They do not support a scenario where transmission occurs primarily through the noon sector.

For solar wind events, there is no clear correlation enhancement along the diagonal, consistent with Figure 3h. Although most bins show weak or no correlation, moderate correlation appears at certain MLT locations, such as when the THEMIS spacecraft is on the dawnside and GMAG stations are on the duskside in Figures 4d and 4e. This MLT dependence may imply a transmission mechanism for solar wind ULF waves, which requires further investigation in the future.

Foreshock ULF waves evolve as they are convected toward the bow shock (e.g., Palmroth et al., 2015). Thus, the wave power that really crosses the bow shock could differ from spacecraft measurements away from the bow

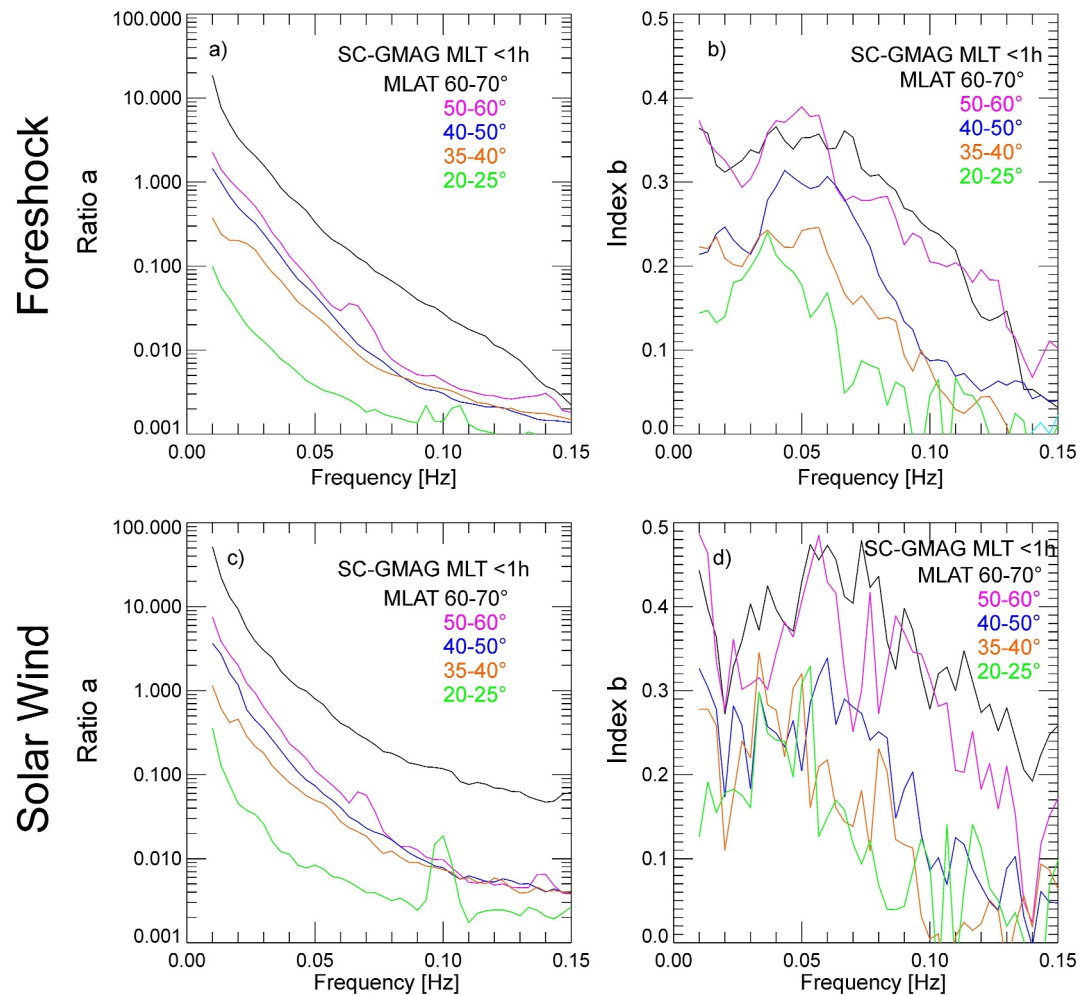


Figure 5. The fitted factors a and b as a function of frequency with magnetic local time separation between the THEMIS spacecraft and ground magnetometers stations less than 1 hr for foreshock events (top) and solar wind events (bottom).

shock. It is expected that wave power measured closer to the bow shock correlates with ground-based wave power better. However, it is difficult to determine distances from the spacecraft to the bow shock. The Merka et al. (2005) bow shock model is used to estimate the distances, but negative distances often appear (even if solar wind speed from OMNI is used to exclude foreshock contamination) indicating large uncertainties compared to realistic (positive) distances. Because of the large uncertainties, we separate events into only two groups based on the median distance. As shown in Figure S5 in Supporting Information S1, the correlation coefficients around the 30s period increase (decrease) by $\lesssim 0.05$ for events close to (far from) the bow shock, compared to Figure 3a. More accurate distance estimates could further highlight the role of distances in correlation.

Next, we examine factors a and b in the relationship $P_m = a \cdot P_u^b$ using linear regression on log-log scales, where P_m is ground-based wave power and P_u is upstream wave power for foreshock events and solar wind events. Figure 5 demonstrates how the fitted factors a and b vary with frequency and MLAT. Factor a indicates the portion of upstream wave power available to the ground (when $b > 0$), while factor b represents how significantly ground-based wave power responds to upstream wave power (e.g., ground-based wave power does not respond when $b = 0$ and varies at the same rate as upstream wave power when $b = 1$). Foreshock and solar wind events show similar factor profiles. Both factors decrease with lower MLAT, suggesting that less wave power is transmitted deeper in the magnetosphere. This is reasonable for wave transmission from the magnetopause as waves could be dissipated during propagation in the magnetosphere through wave-particle interaction and energy loss in the ionosphere. Additionally, both factors decrease with increasing frequency, suggesting that the transmission may be more difficult for higher-frequency waves. Factor b also shows a bump at 0.03–0.06 Hz.

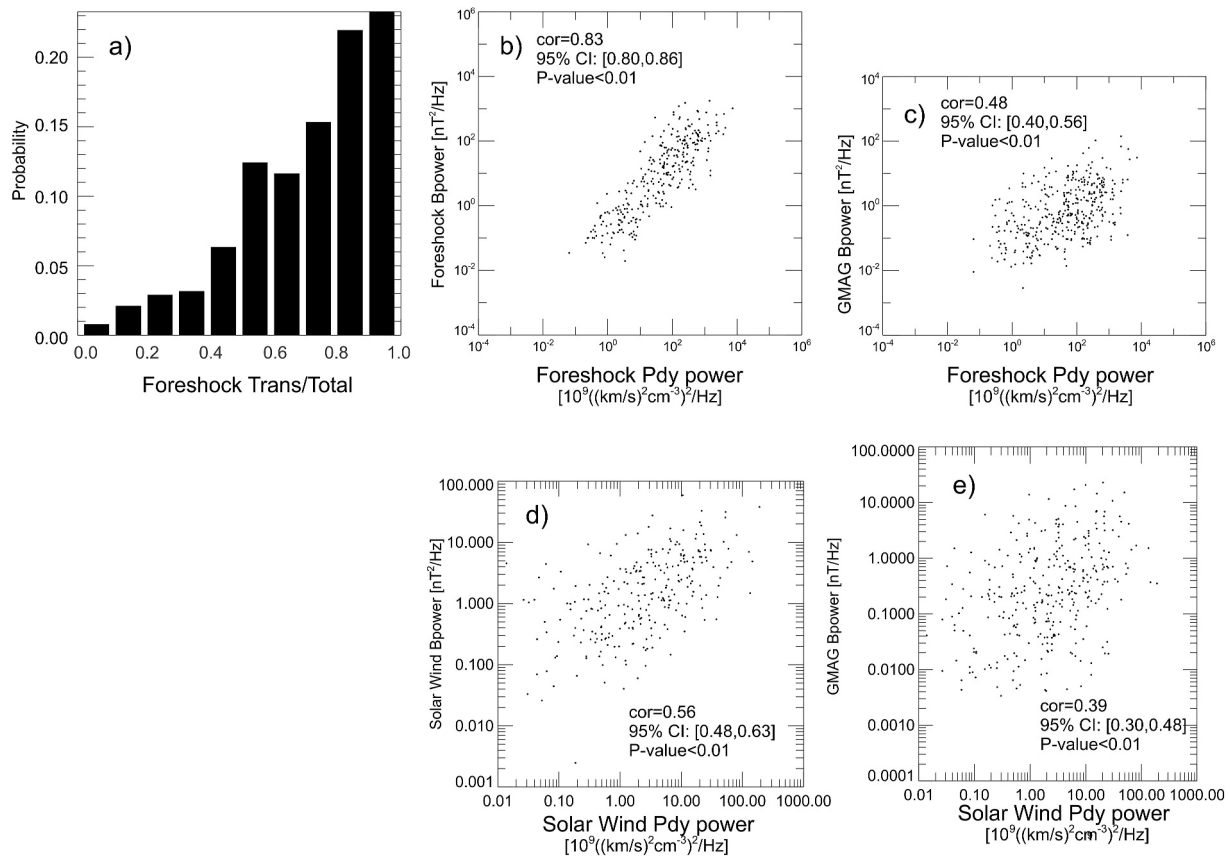


Figure 6. Using the same data set as that in Figure 2a (at 0.04 Hz and 50–60° magnetic latitudes with magnetic local time separation between the THEMIS spacecraft and ground magnetometers stations less than 1 hr), panel (a) shows the probability distribution of the ratio of transverse wave power to total wave power for the foreshock ultralow frequency (ULF) wave. Panels (b) and (c) show the dynamic pressure (Pdy) wave power versus foreshock and ground-based ULF magnetic wave power, respectively. Panels (d) and (e) are in the same format as panels (b) and (c) except for solar wind dynamic pressure wave power. Spearman correlation coefficient, 95% confidence interval, and *P*-value are labeled in each panel.

Standing wave modes at ~0.03–0.06 Hz may enhance the transmission efficiency to the ground and contribute to this bump (Hartinger et al., 2023; Takahashi & Anderson, 1992).

How foreshock ULF waves cross the magnetopause is still unclear. Since compressional field oscillations can directly cross the magnetopause, we separate magnetic fields into compressional and transverse components using local field-aligned coordinates. Figure 6a shows the probability distributions of transverse wave power over total wave power at 0.04 Hz for foreshock ULF waves, using the same data set as Figure 2a. Foreshock ULF waves tend to have larger transverse components than compressional components (the probability distributions are similar at other frequencies around 0.04 Hz). The correlation coefficient between the transverse components of foreshock ULF waves and total wave power measured by GMAG stations is similar to that in Figure 2a, whereas the correlation coefficient decreases when using the compressional components. Our results do not support direct transmission of compressional components. One possible cause could be that the bow shock transmission and propagation in the magnetosheath might redistribute transverse and compressional components.

Foreshock ULF waves are typically associated with significant density and velocity fluctuations (e.g., Figures 1b and 1c). Figure 6b shows a strong correlation between dynamic pressure wave power and foreshock magnetic wave power, with a Spearman correlation coefficient of 0.83 at 0.04 Hz. Figure 6c shows that the correlation coefficient between dynamic pressure wave power and ground-based magnetic wave power is 0.48, which is slightly less than that in Figure 2a (covered by uncertainty range; similar for other MLAT). This correlation suggests a possibility that foreshock ULF waves might disturb the magnetopause through their dynamic pressure oscillations to locally excite magnetospheric ULF waves. This process could be similar to how foreshock

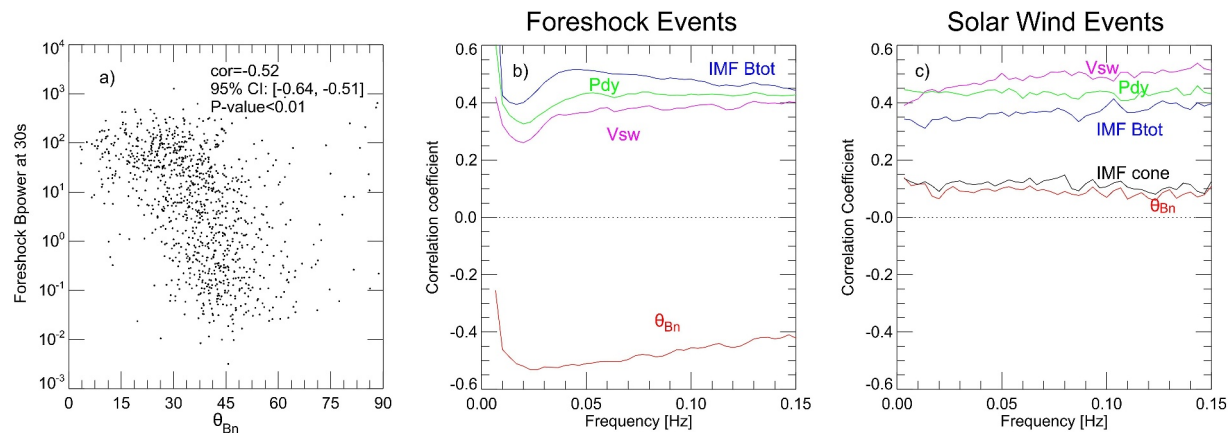


Figure 7. (a) Foreshock ultralow frequency (ULF) wave power versus local θ_{Bn} at 0.033 Hz. (b) The Spearman correlation coefficients between foreshock ULF wave power and local θ_{Bn} , interplanetary magnetic field strength (Btot), solar wind speed (Vsw), and dynamic pressure (Pdy) as a function of frequency. Panel (c) is in the same format as Panel (b) except for solar wind wave power.

transients (see review by Zhang et al. (2022)) locally disturb the magnetosphere (e.g., Liu et al., 2022; Sibeck et al., 1999; Wang et al., 2021). Further observations and simulations are needed to investigate this.

In comparison, solar wind dynamic pressure wave power is less correlated with solar wind magnetic wave power (Figure 6d) compared with foreshock waves, probably because multiple wave modes are mixed. The correlation between solar wind dynamic pressure wave power and ground-based magnetic wave power (Figure 6e) is slightly stronger than that for solar wind magnetic wave power in Figure 2c, suggesting the role of dynamic pressure disturbances.

How the magnetopause is disturbed could affect the wave properties observed by GMAG stations. If we use only the north-south or east-west component from GMAG stations to correlate with foreshock ULF waves (at 0.036 Hz using GMAG stations with MLAT of 50–60° and MLT separation from spacecraft less than 1 hr), the two Spearman correlation coefficients are similar (~ 0.49), slightly smaller than that using all three components (~ 0.51). If we use a vertical component, the correlation coefficient drops to ~ 0.42 . If we use both north-south and east-west components, the correlation coefficient is almost the same as that using all three components. Thus, it indicates that the combination of north-south and east-west components dominates the ground responses (Figure S6 in Supporting Information S1 shows probability distribution of three wave power components). This result suggests that the ground responses are not purely toroidal or poloidal modes (e.g., Klimushkin et al., 2004).

3.2. Upstream Parameter Dependence

Previous statistical studies have identified that magnetospheric Pc3–4 wave power is correlated with IMF cone angle, IMF strength, and solar wind velocity (e.g., Singer et al., 1977; Takahashi et al., 1984). We reassess these dependencies to determine whether they are due to foreshock ULF waves. Figure 7a shows that foreshock wave power at 30s is negatively correlated with local bow shock θ_{Bn} , as expected (e.g., Kajdič et al., 2021). Figure 7b shows that the Spearman correlation coefficient between the foreshock wave power and θ_{Bn} (red line) peaks at ~ 0.02 – 0.03 Hz.

Foreshock wave power is also correlated with the IMF strength (blue in Figure 7b), probably because the maximum amplitudes of foreshock ULF waves are limited by the background IMF strength. The Spearman correlation coefficient increases with decreasing frequency except for a dip at ~ 0.02 Hz. This dip is likely due to the lower peak frequency of wave power at weaker IMF strength (e.g., Takahashi et al., 1984), which increases wave power at lower frequency for weaker IMF strength and thus weakens the correlation (see Figure S7 in Supporting Information S1). Additionally, foreshock wave power is correlated with the solar wind speed (magenta in Figure 7b), but the correlation is weaker than that with the dynamic pressure (green; the difference is comparable to 95% confidence interval), suggesting that the dynamic pressure is a more important factor. Larger dynamic pressure or kinetic energy of solar wind ions leads to larger foreshock ion energy, the energy source of foreshock ULF waves. The correlation coefficients with the solar wind speed and dynamic pressure also show a

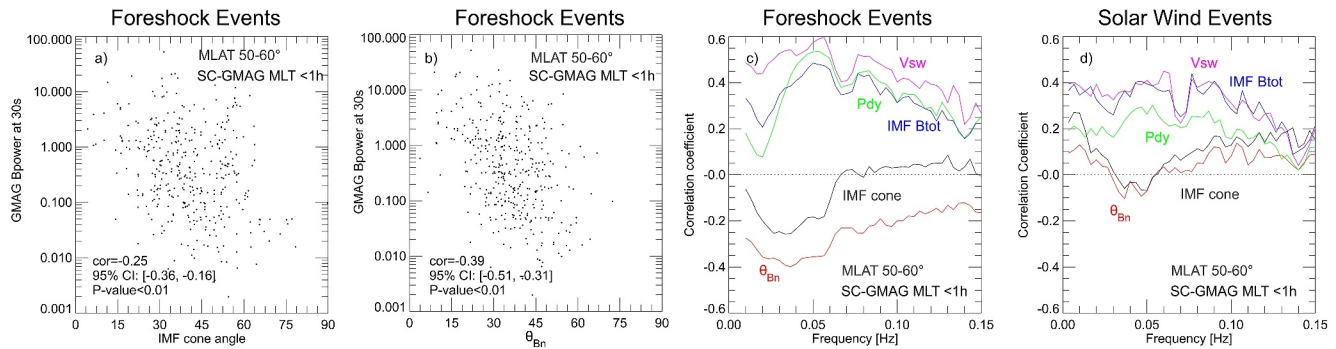


Figure 8. (a) Ground-based ultralow frequency (ULF) wave power during foreshock time intervals versus interplanetary magnetic field (IMF) cone angle at 0.033 Hz. (b) Ground-based ULF wave power during foreshock time intervals versus local θ_{Bn} at 0.033 Hz. (c) The Spearman correlation coefficients between ground-based ULF wave power during foreshock time intervals and IMF cone angle, local θ_{Bn} , IMF strength, solar wind speed, and dynamic pressure, as a function of frequency. Panel (d) is in the same format as Panel (c) except for solar wind time intervals.

dip at ~ 0.02 Hz. These dips are also likely caused by the frequency dependence on IMF strength, as solar wind speed and dynamic pressure are correlated with IMF strength with correlation coefficients of 0.41 and 0.58, respectively. (We do not consider the role of distances to the bow shock because of large uncertainties and their dependence on dynamic pressure.) In contrast, solar wind wave power shows a stronger dependence on the solar wind speed than dynamic pressure and IMF strength and no dependence on θ_{Bn} or IMF cone angle (Figure 7c).

As for ground-based Pc3-4 wave power during foreshock time intervals, it is correlated with the IMF cone angle (Figure 8a) at frequencies of ~ 0.02 – 0.05 Hz (black in Figure 8c), consistent with previous statistical studies (e.g., Takahashi et al., 1984). For each GMAG station, when there is a THEMIS spacecraft located within ± 1 hr MLT of the station, we use θ_{Bn} measured by that spacecraft to correlate with ground-based wave power. The correlation shown in Figure 8b and the red line in Figure 8c improves compared to that shown in Figure 8a and the black line in Figure 8c. If the MLT separations between the THEMIS spacecraft and GMAG stations are increased from ± 1 to ± 6 hr to obtain θ_{Bn} , the correlation decreases by ~ 0.1 , consistent with the results shown in Figure 3d. These results again indicate that foreshock ULF waves are more likely transmitted from the local bow shock than from the subsolar point (where IMF cone angle equals θ_{Bn}).

Ground-based Pc3-4 wave power is also correlated with the IMF strength (blue in Figure 8c), consistent with previous studies (e.g., Takahashi et al., 1984). The profile of the correlation coefficient is similar to that in Figure 7b. Thus, this correlation is likely due to foreshock ULF wave properties. Additionally, unlike in Figure 7b, the correlation with the solar wind speed (magenta) is stronger than that with the dynamic pressure (green). This stronger dependence on the solar wind speed suggests that the KH instability may contribute to magnetospheric Pc3-4 waves simultaneously with foreshock ULF waves, especially at lower frequencies (consistent with the fact that the KH instability is an important factor controlling wave amplitude at Pc5 frequency). Another possible contributor is foreshock transients and magnetosheath jets. These shock-generated transients tend to form under fast solar wind speed (e.g., Liu et al., 2017; Plaschke et al., 2013) and can drive magnetospheric ULF waves (e.g., Hartinger et al., 2013; Wang et al., 2022; Zhao et al., 2017).

In comparison, ground-based ULF wave power during solar wind time intervals does not correlate with θ_{Bn} or IMF cone angle (Figure 8d). It also shows a stronger correlation with the solar wind speed than dynamic pressure, similar to Figure 7c. It is possible that solar wind wave transmission may also contribute to the stronger dependence on the solar wind speed than dynamic pressure in Figure 8c.

4. Discussion

Previously, foreshock ULF waves were often thought to be transmitted through the subsolar point, possibly due to the dependence on the IMF cone angle (e.g., Greenstadt & Olson, 1976; Russell et al., 1983; Takahashi et al., 1984). However, our results show that foreshock ULF waves should be more likely transmitted from the local bow shock than from the subsolar point, especially more frequently on the dawnside where the foreshock tends to occur preferentially. This is based on our findings that: (a) the correlation between foreshock and ground-based ULF wave power is stronger when the THEMIS spacecraft and GMAG stations are closer in MLT

(preferentially within ± 1 hr); and (b) ground-based Pc3-4 wave power shows a stronger dependence on the local bow shock θ_{Bn} measured by the THEMIS spacecraft within ± 1 hr MLT than the IMF cone angle (equal to θ_{Bn} at the subsolar bow shock). Additionally, broader-range transmission across a few hours of MLT could coexist, as suggested by Figure 4. Further analysis will be necessary to clarify the underlying physical transmission mechanisms.

Next, we discuss the limitations or potential improvements of our statistical analysis. First, we did not consider the time needed for wave transmission and propagation. In the magnetosheath, the waves could be convected by the tailward magnetosheath flow. The convection effect is stronger farther away from the subsolar point under faster solar wind speed. Here, we conduct a simple estimate. For 3-min convection at a speed of ~ 100 km/s in the azimuthal direction (estimated based on the average solar wind speed component tangential to the bow shock normal in our data set), the distance is $\sim 2.8 R_E$ corresponding to ~ 1 hr MLT at a radial distance of $10 R_E$. However, 1 hr MLT bin size for spacecraft-GMAG station separation is used to guarantee sufficient data numbers, causing difficulties in identifying this convection effect. In the future, more GMAG data sets (e.g., from SuperMAG) could be used to provide better MLT (as well as MLAT) resolution.

Additionally, we compare the wave power spectra upstream and downstream at the same time. If we consider the time delay due to wave propagation, the correlation coefficients could be improved. However, the time delay should vary for different events, causing difficulties in performing a statistical analysis. To determine the best time delay, we need to use a short time step for the moving window to calculate all the wave power spectra within each foreshock time interval at each GMAG station, leading to a much larger amount of calculation. Thus, the time delay effect may require a better method in the future.

Second, we compare wave power across events at the same frequency. However, foreshock ULF wave power could peak at the frequency determined by the ion cyclotron frequency. Further work could consider normalizing the frequency to the ion cyclotron frequency, which may improve the correlation coefficients.

Third, we only consider foreshock ULF waves in the equatorial plane in which THEMIS orbits. When the ion foreshock extends to a high latitude, we expect that foreshock ULF waves could be transmitted locally and possibly enter the magnetosphere through the cusp (e.g., Engebretson et al., 1987). Cluster observations could be used to examine wave transmission off the equatorial plane.

Fourth, the properties of foreshock ULF waves could vary when they cross the bow shock and propagate in the magnetosheath. There are also locally generated waves in the magnetosheath (Lacombe & Belmont, 1995), which may also contribute to magnetospheric ULF waves. Therefore, statistical studies between the foreshock and the magnetosheath and between the magnetosheath and the magnetosphere are needed.

Fifth, field line resonances are included in our database, which can weaken the correlation with foreshock ULF waves (e.g., Veró et al., 1998). To minimize effects from field line resonances, we could use magnetosphere models to estimate the frequencies of field line resonances at each GMAG station (e.g., Archer et al., 2015; Wild et al., 2005) and exclude wave power at these frequencies.

Sixth, our results suggest that the KH instability could contribute simultaneously; thus, the correlation could improve if we separate the contribution from the KH instability and foreshock ULF waves. In the future, we could fix the solar wind speed to exclude variations from the KH instability. Such analysis, however, requires a larger database.

Finally, we use ground-based ULF wave power to remotely infer the magnetospheric ULF wave power. The relationship between the two wave powers, however, is modulated by many factors, such as the modes of ULF waves and the properties of the ionosphere, atmosphere, and ground (e.g., review by Southwood & Hughes, 1983). For example, the ionospheric conductivity affects Pederson currents and Hall currents that in turn determine the magnetic field perturbations observed on the ground. If magnetospheric ULF waves are Alfvén mode carrying field-aligned currents, the polarization is rotated 90° above and below the ionosphere. Ionospheric screening can also filter short azimuthal wavelength ($< \sim 120$ km), causing no or attenuated signals on the ground. Non-resonant coupling between compressional and Alfvén modes can result in field-aligned currents throughout the magnetosphere, which modify ground magnetic field perturbations (Archer et al., 2023). Thus, to fully address wave transmission from the foreshock to the magnetosphere and to the ground, simultaneous spacecraft observations in the magnetosphere will be needed in the future.

5. Summary

Using conjunctions between the THEMIS spacecraft and GMAG stations, we perform a statistical study between foreshock ULF wave power and ground-based Pc3–4 wave power for the first time. We summarize our results as follows. (a) The contribution from foreshock ULF wave power to ground-based ULF wave power follows a power-law relationship, $P_m = a \cdot P_f^b$. (b) The correlation coefficients exceed 0.5 at ~ 0.03 – 0.06 Hz, the frequency range of foreshock 30s waves, across a wide MLAT range. (c) The MLT dependence of correlation coefficients does not favor transmission from the subsolar point. (d) The correlation coefficients decrease with larger MLT separation between the THEMIS spacecraft and GMAG stations. (e) The fitted factors a and b decrease with lower MLAT suggesting less and weaker power transmission deeper in the magnetosphere for both foreshock and solar wind ULF waves. (f) Foreshock ULF waves might be transmitted across the magnetopause through their dynamic pressure oscillations. (g) Ground-based Pc3–4 wave power shows a stronger dependence on the local θ_{Bn} (within ± 1 hr MLT) than on the IMF cone angle. (h) Ground-based Pc3–4 wave power shows an extra dependence on the solar wind speed compared to foreshock ULF wave power, suggesting additional contributors such as the KH instability and shock-generated transients.

Our results suggest that the foreshock ULF waves are more likely transmitted from the local bow shock (preferentially within ± 1 hr MLT) into the magnetosphere (more frequently on the dawnside) than from the subsolar point. Our results also suggest the possible co-existence of broader-range transmission across a few hours of MLT. There are still many unknowns, such as propagation and evolution of transmitted waves in the magnetosheath, contribution from magnetosheath-generated waves, transmission mechanism across the magnetopause, and propagation in the magnetosphere. More comprehensive studies are needed to complete the full picture of wave transmission from the foreshock.

Data Availability Statement

THEMIS and GMAG data sets (including station list) are available at NASA's Coordinated Data Analysis Web (CDAWeb, <https://cdaweb.gsfc.nasa.gov/cgi-bin/eval1.cgi>). The SPEDAS software (see Angelopoulos et al. (2019)) is available at <https://themis.ssl.berkeley.edu/software.shtml>.

Acknowledgments

T. Z. L. is partially supported by NSF award AGS-2247760 and NASA Grants 80NSSC23K0086 and 80NSSC25K7684. S.D. is supported by NASA Grant 80NSSC20K0801. M.D.H. is supported by NSF award AGS-2307204. K.Z. is supported by NASA Grant 80NSSC25K7684 and NSF award AGS-2420710. SR acknowledges funding from NASA DRIVE Science Center for Geospace Storms (CGS)—80NSSC22M0163, and Johns Hopkins University Applied Physics Laboratory independent R&D fund. T. Z. L. acknowledges discussion with ISSI team led by Primož Kajdic. We acknowledge the NASA THEMIS contract NAS5-02099, the SPEDAS team and NASA's Coordinated Data Analysis Web. We thank K. H. Glassmeier and U. Auster and W. Baumjohann for the use of the THEMIS/FGM data provided under the lead of the Technical University of Braunschweig and with financial support through the German Ministry for Economy and Technology and the German Center for Aviation and Space (DLR) under contract 50 OC 0302. We also thank the late C. W. Carlson and J. P. McFadden for the use of THEMIS/ESA data. We thank several GMAG networks for measurements used in this study, including THEMIS GBO, CARISMA, and USGS.

References

- Angelopoulos, V. (2008). The THEMIS mission. *Space Science Reviews*, 141(1–4), 5–34. <https://doi.org/10.1007/s11214-008-9336-1>
- Angelopoulos, V., Cruce, P., Drozdov, A., Grimes, E. W., Hatzigeorgiou, N., King, D. A., et al. (2019). The space physics environment data analysis system (SPEDAS) [Software]. *Space Science Reviews*, 215(1), 9. <https://doi.org/10.1007/s11214-018-0576-4>
- Archer, M. O., Hartinger, M. D., Rastätter, L., Southwood, D. J., Heyns, M., Eggington, J. W. B., et al. (2023). Auroral, ionospheric and ground magnetic signatures of magnetopause surface modes. *Journal of Geophysical Research: Space Physics*, 128(3), e2022JA031081. <https://doi.org/10.1029/2022JA031081>
- Archer, M. O., Hartinger, M. D., Walsh, B. M., Plaschke, F., & Angelopoulos, V. (2015). Frequency variability of standing Alfvén waves excited by fast mode resonances in the outer magnetosphere. *Geophysical Research Letters*, 42(23), 10150–10159. <https://doi.org/10.1002/2015GL066683>
- Auster, H. U., Glassmeier, K. H., Magnes, W., Aydogar, O., Baumjohann, W., Constantinescu, D., et al. (2008). The THEMIS fluxgate magnetometer. *Space Science Reviews*, 141(1–4), 235–264. <https://doi.org/10.1007/s11214-008-9365-9>
- Bentley, S. N., Watt, C. E. J., Owens, M. J., & Rae, I. J. (2018). ULF wave activity in the magnetosphere: Resolving solar wind interdependencies to identify driving mechanisms. *Journal of Geophysical Research: Space Physics*, 123(4), 2745–2771. <https://doi.org/10.1002/2017JA024740>
- Burgess, D., Möbius, E., & Scholer, M. (2012). Ion acceleration at the Earth's bow shock. In *Space Science Reviews*. Springer Science and Business Media LLC. <https://doi.org/10.1007/s11214-012-9901-5>
- Clausen, L. B. N., Yeoman, T. K., Fear, R. C., Behlke, R., Lucek, E. A., & Engebretson, M. J. (2009). First simultaneous measurements of waves generated at the bow shock in the solar wind, the magnetosphere and on the ground. In *Annales Geophysicae*. Copernicus GmbH. <https://doi.org/10.5194/angeo-27-357-2009>
- Eastwood, J. P., Lucek, E. A., Mazelle, C., Meziane, K., Narita, Y., Pickett, J., & Treumann, R. A. (2005). The foreshock. In *Space Science Reviews*. Springer Science and Business Media LLC. <https://doi.org/10.1007/s11214-005-3824-3>
- Engebretson, M. J., Zanetti, L. J., Potemra, T. A., Baumjohann, W., Lühr, H., & Acuna, M. H. (1987). Simultaneous observation of Pc 3–4 pulsations in the solar wind and in the Earth's magnetosphere. *Journal of Geophysical Research*, 92(A9), 10053–10062. <https://doi.org/10.1029/JA092iA09p10053>
- Eriksson, P. T. I., Walker, A. D. M., & Stephenson, J. A. E. (2006). A statistical correlation of Pc5 pulsations and solar wind pressure oscillations. *Advances in Space Research*, 38(8), 1763–1771. <https://doi.org/10.1016/j.asr.2005.08.023>
- Golikov, Y. Y., Plyasova-Bakunina, T. A., Troitskaya, V. A., Chernikov, A. A., & Plastovalov, V. V. (1983). Where do solar wind controlled micro-pulsations originate. *Planetary and Space Science*, 28, 535–543. [https://doi.org/10.1016/0032-0633\(80\)90034-3](https://doi.org/10.1016/0032-0633(80)90034-3)
- Greenstadt, E. W., & Olson, J. V. (1976). Pc 3, 4 activity and interplanetary field orientation. *Journal of Geophysical Research*, 81(34), 5911–5920. <https://doi.org/10.1029/JA081i034p05911>
- Hartinger, M. D., Elsdén, T., Archer, M. O., Takahashi, K., Wright, A. N., Artemyev, A., et al. (2023). Properties of Magnetohydrodynamic normal modes in the Earth's magnetosphere. *Journal of Geophysical Research: Space Physics*, 128(12), e2023JA031987. <https://doi.org/10.1029/2023JA031987>

- Hartering, M. D., Turner, D. L., Plaschke, F., Angelopoulos, V., & Singer, H. (2013). The role of transient ion foreshock phenomena in driving Pc5 ULF wave activity. *Journal of Geophysical Research: Space Physics*, 118(1), 299–312. <https://doi.org/10.1029/2012JA018349>
- Jacobs, J. A., Kato, Y., Matsushita, S., & Troitskaya, V. A. (1964). Classification of geomagnetic micropulsations. *Journal of Geophysical Research*, 69(1), 180–181. <https://doi.org/10.1029/JZ069i001p00180>
- Kajdić, P., Pfau-Kempf, Y., Turc, L., Dimmock, A. P., Palmroth, M., Takahashi, K., et al. (2021). ULF wave transmission across collisionless shocks: 2.5D local hybrid simulations. *Journal of Geophysical Research: Space Physics*, 126(11), e2021JA029283. <https://doi.org/10.1029/2021JA029283>
- Klimushkin, D. Y., Mager, P. N., & Glassmeier, K.-H. (2004). Toroidal and poloidal Alfvén waves with arbitrary azimuthal wavenumbers in a finite pressure plasma in the Earth's magnetosphere. *Annals of Geophysics*, 22(1), 267–287. <https://doi.org/10.5194/angeo-22-267-2004>
- Lacombe, C., & Belmont, G. (1995). Waves in the Earth's magnetosheath: Observations and interpretations. In *Advances in Space Research*. Elsevier BV. [https://doi.org/10.1016/0273-1177\(94\)00113-f](https://doi.org/10.1016/0273-1177(94)00113-f)
- Lanzerotti, L. J., Medford, L. V., MacLennan, C. G., Hasegawa, T., Acuna, M. H., & Dolce, S. R. (1981). Polarization characteristics of hydromagnetic waves at low geomagnetic latitudes. *Journal of Geophysical Research*, 86(A7), 5500–5506. <https://doi.org/10.1029/JA086iA07p05500>
- Liu, T. Z., Angelopoulos, V., Hietala, H., & Wilson, L. B. III. (2017). Statistical study of particle acceleration in the core of foreshock transients. *Journal of Geophysical Research: Space Physics*, 122(7), 7197–7208. <https://doi.org/10.1002/2017JA024043>
- Liu, T. Z., Wang, C.-P., Wang, X., Angelopoulos, V., Zhang, H., Lu, X., & Lin, Y. (2022). Magnetospheric field-aligned current generation by foreshock transients: Contribution by flow vortices and pressure gradients. *Journal of Geophysical Research: Space Physics*, 127(11), e2022JA030700. <https://doi.org/10.1029/2022JA030700>
- McFadden, J. P., Carlson, C. W., Larson, D., Angelopoulos, V., Ludlam, M., Abiad, R., et al. (2008). The THEMIS ESA plasma instrument and in-flight calibration. *Space Science Reviews*, 141(1–4), 277–302. <https://doi.org/10.1007/s11214-008-9440-2>
- Menk, F. W. (2011). *Magnetospheric ULF waves: A review. The dynamic magnetosphere*. Springer Netherlands. https://doi.org/10.1007/978-94-007-0501-2_13
- Merka, J., Szabo, A., Slavin, J. A., & Peredo, M. (2005). Three-dimensional position and shape of the bow shock and their variation with upstream Mach numbers and interplanetary magnetic field orientation. *Journal of Geophysical Research*, 110(A4), A04202. <https://doi.org/10.1029/2004JA010944>
- Palmroth, M., Archer, M., Vainio, R., Hietala, H., Pfau-Kempf, Y., Hoilijoki, S., et al. (2015). ULF foreshock under radial IMF: THEMIS observations and global kinetic simulation Vlasior results compared. *Journal of Geophysical Research: Space Physics*, 120(10), 8782–8798. <https://doi.org/10.1002/2015JA021526>
- Plaschke, F., Hietala, H., & Angelopoulos, V. (2013). Anti-sunward high-speed jets in the subsolar magnetosheath. *Annals of Geophysics*, 31(10), 1877–1889. <https://doi.org/10.5194/angeo-31-1877-2013>
- Russell, C. T., Chi, P. J., Dearborn, D. J., Ge, Y. S., Kuo-Tiong, B., Means, J. D., et al. (2009). THEMIS ground-based magnetometers. In J. L. Burch & V. Angelopoulos (Eds.), *The THEMIS Mission*. Springer. https://doi.org/10.1007/978-0-387-89820-9_17
- Russell, C. T., & Hoppe, M. M. (1981). The dependence of upstream wave periods on the interplanetary magnetic field strength. *Geophysical Research Letters*, 8(6), 615–617. <https://doi.org/10.1029/GL008i006p00615>
- Russell, C. T., & Hoppe, M. M. (1983). Upstream waves and particles. *Space Science Reviews*, 34, 155–172. https://doi.org/10.1007/978-94-009-7096-0_12
- Russell, C. T., Luhmann, J. G., Odera, T. J., & Stuart, W. F. (1983). The rate of occurrence of dayside Pc 3,4 pulsations: The L-value dependence of the IMF cone angle effect. *Geophysical Research Letters*, 10(8), 663–666. <https://doi.org/10.1029/GL010i008p00663>
- Shue, J.-H., Song, P., Russell, C. T., Steinberg, J. T., Chao, J. K., Zastenker, G., et al. (1998). Magnetopause location under extreme solar wind conditions. *Journal of Geophysical Research*, 103(A8), 17691–17700. <https://doi.org/10.1029/98JA01103>
- Sibeck, D. G., Borodkova, N. L., Schwartz, S. J., Owen, C. J., Kessel, R., Kokubun, S., et al. (1999). Comprehensive study of the magnetospheric response to a hot flow anomaly. *Journal of Geophysical Research*, 104(A3), 4577–4593. <https://doi.org/10.1029/1998JA900021>
- Singer, H. J., Russell, C. T., Kivelson, M. G., Greenstadt, E. W., & Olson, J. V. (1977). Evidence for the control of Pc 3,4 magnetic pulsations by the solar wind velocity. *Geophysical Research Letters*, 4(9), 377–379. <https://doi.org/10.1029/GL004i009p00377>
- Southwood, D. J., & Hughes, W. J. (1983). Theory of hydromagnetic waves in the magnetosphere. *Space Science Reviews*, 35(4), 301–366. <https://doi.org/10.1007/BF00169231>
- Stephenson, J. A. E., & Walker, A. D. M. (2002). HF radar observations of Pc5 ULF pulsations driven by the solar wind. *Geophysical Research Letters*, 29(9). <https://doi.org/10.1029/2001gl014291>
- Takahashi, K., & Anderson, B. J. (1992). Distribution of ULF energy ($f < 80$ mHz) in the inner magnetosphere: A statistical analysis of AMPTE cce magnetic field data. *Journal of Geophysical Research*, 97(A7), 10751–10773. <https://doi.org/10.1029/92JA00328>
- K. Takahashi, P. J. Chi, R. E. Denton, & R. L. Lysak (Eds.) (2006). *Magnetospheric ULF waves: Synthesis and new directions. Geophysical Monograph Series*. American Geophysical Union. <https://doi.org/10.1029/gm169>
- Takahashi, K., McPherron, R. L., & Terasawa, T. (1984). Dependence of the spectrum of Pc 3–4 pulsations on the interplanetary magnetic field. *Journal of Geophysical Research*, 89(A5), 2770–2780. <https://doi.org/10.1029/JA089iA05p02770>
- Takahashi, K., Turc, L., Kilpua, E., Takahashi, N., Dimmock, A., Kajdić, P., et al. (2021). Propagation of ultralow-frequency waves from the ion foreshock into the magnetosphere during the passage of a magnetic cloud. *Journal of Geophysical Research: Space Physics*, 126(2), e2020JA028474. <https://doi.org/10.1029/2020JA028474>
- Turc, L., Roberts, O. W., Verscharen, D., Dimmock, A. P., Kajdić, P., Palmroth, M., et al. (2023). Transmission of foreshock waves through Earth's bow shock. *Nature Physics*, 19(1), 78–86. <https://doi.org/10.1038/s41567-022-01837-z>
- Turc, L., Zhou, H., Tarvus, V., Ala-Lahti, M., Battarbee, M., Pfau-Kempf, Y., et al. (2022). A global view of Pc3 wave activity in near-Earth space: Results from hybrid-Vlasov simulations. In *Frontiers in Astronomy and Space Sciences*. Frontiers Media SA. <https://doi.org/10.3389/fspas.2022.989369>
- Verö, J., Lühr, H., Vellante, M., Best, I., Štefšćik, J., Miletits, J. C., et al. (1998). Upstream waves and field line resonances: Simultaneous presence and alternation in Pc3 pulsation events. In *Annales Geophysicae*. Copernicus GmbH. <https://doi.org/10.1007/s00585-997-0034-1>
- Verzariu, P. (1973). Reflection and refraction of hydromagnetic waves at the magnetopause. In *Planetary and Space Science*. Elsevier BV. [https://doi.org/10.1016/0032-0633\(73\)90194-3](https://doi.org/10.1016/0032-0633(73)90194-3)
- Wang, B., Nishimura, Y., Hietala, H., & Angelopoulos, V. (2022). Investigating the role of magnetosheath high-speed jets in triggering dayside ground magnetic ultra-low frequency waves. *Geophysical Research Letters*, 49(22), e2022GL099768. <https://doi.org/10.1029/2022GL099768>
- Wang, C.-P. W. X., Liu, T. Z., & Lin, Y. (2021). Impact of foreshock transients on the Flank magnetopause and magnetosphere and the ionosphere. *Front. Astron. Space Sci.*, 8, 751244. <https://doi.org/10.3389/fspas.2021.751244>

- Wild, J. A., Yeoman, T. K., & Waters, C. L. (2005). Revised time-of-flight calculations for high-latitude geomagnetic pulsations using a realistic magnetospheric magnetic field model. *Journal of Geophysical Research*, 110(A11), A11206. <https://doi.org/10.1029/2004JA010964>
- Wilson, L. B., III. (2016). Low frequency waves at and upstream of collisionless shocks. In A. Keiling, D.-H. Lee, & V. Nakariakov (Eds.), *Low-frequency waves in Space plasmas*. <https://doi.org/10.1002/9781119055006.ch16>
- Wolfe, A., Lanzerotti, L., & MacLennan, C. (1980). Dependence of hydromagnetic energy spectra on solar wind velocity and interplanetary magnetic field direction. *Journal of Geophysical Research*, 85(A1), 114–118. <https://doi.org/10.1029/JA085iA01p00114>
- Zhang, H., Zong, Q., Connor, H., Delamere, P., Facskó, G., Han, D., et al. (2022). Dayside transient phenomena and their impact on the magnetosphere and ionosphere. *Space Science Reviews*, 218(5), 40. <https://doi.org/10.1007/s11214-021-00865-0>
- Zhao, L. L., Zhang, H., & Zong, Q. G. (2017). Global ULF waves generated by a hot flow anomaly. *Geophysical Research Letters*, 44(11), 5283–5291. <https://doi.org/10.1002/2017GL073249>